Materials & Design 242 (2024) 113014

Contents lists available at ScienceDirect

Materials & Design

journal homepage: www.elsevier.com/locate/matdes

Micro and nanostructured carbon-phenolic ablators modified by PVP addition

Laura Paglia [a,b,*], Rita Bottacchiari [a,b], Flavio Cognigni [c], Sara Cerra [d], Virgilio Genova [a,b], Marco Rossi [c], Ilaria Fratoddi [d,e], Francesco Marra [a,b], Giovanni Pulci [a,b]

[a] Department of Chemical Engineering Materials Environment, Sapienza University of Rome, Via Eudossiana 18, 00184 Rome, Italy
[b] INSTM Reference Laboratory for Materials and Surface Treatments, Italy
[c] Department of Basic and Applied Sciences for Engineering (SBAI), Sapienza University of Rome, Via Antonio Scarpa 14, Rome, 00161, Italy
[d] Department of Chemistry, Sapienza University of Rome, piazzale Aldo Moro 5, 00185 Rome, Italy
[e] Research Center for Applied Sciences to the Safeguard of Environment and Cultural Heritage (CIABC), Sapienza University of Rome, Piazzale Aldo Moro 5, 00185 Rome, Italy

ARTICLE INFO

Keywords:
Polimer-matrix composites
Microstructures
Thermal analysis
Cure

ABSTRACT

Carbon-phenolic ablators can efficiently protect space vehicles from the extreme temperatures typical of the reentry phase in a planet's atmosphere. Their performances are attributed to the low thermal conductivity and to the decomposition of the phenolic resin. These phenomena are strongly influenced by the materials microstructure. In the present work, standard and polyvinylpyrrolidone (PVP)-modified carbon-phenolic ablators were manufactured and characterized: the influence of PVP on the final microstructure and chemistry of the ablators was studied through SEM-EDS, X-ray Microscopy (XRM) analysis and FTIR technique; the mechanical properties were evaluated through compression tests on virgin and charred samples while ablative performance of the ablators were evaluated with an oxyacetylene flame exposure test. Weak bonds between phenolic resin chains and PVP were observed. The microstructure of the ablators, both before and after the exposure to the oxyacetylene flame, is strongly influenced by the PVP addition, furthermore the addition of 10 and 20 %wt of PVP can guarantee a reduction of about 30 % of the back temperature during the oxyacetylene flame test with respect to the standard carbon-phenolic ablator. Compression tests on the manufactured ablators enlighten also an improvement in the mechanical properties for PVP-enriched ablators, in particular considering their charred state.

1. Introduction

During the atmospheric reentry of a space vehicle, the friction between the vehicle surface and the atmosphere molecules causes an overheating which can damage the vehicle structure, the payload and/or the crew [1–3]. For this reason, highly efficient thermal shields are mandatory: low density carbon phenolic ablative materials, such as the NASA-designed PICA [4], were successfully used in interplanetary missions (Mars 2020 and MRS laboratory 2012) as well as for the reentry on the Earth from the International Space Station (Dragon SpaceX) [3,5,6]. These materials are designed to promote several mechanisms of heat dissipation, allowing them to withstand the huge heat fluxes typical of ballistic atmospheric reentries [3,7]. Low density carbon-phenolic ablators are composite materials having a phenolic resin matrix and carbon fibers as reinforcement. Generally, a carbon felt is impregnated with a small amount of phenolic resin so that the final composite is highly porous, thus exhibiting excellent thermal insulation properties. When temperatures exceed 300 °C [8] the phenolic resin begins to undergo the endothermic reaction of pyrolysis, decomposing into pyrolysis gasses and a solid and porous carbonaceous residue [8,9]. The pyrolysis gasses warm up absorbing heat and, because of the pressure gradient with the external surface, they flow through the open porosities of the material into the boundary layer. In this way, the pyrolysis gasses form a barrier hindering the convective exchange and therefore reducing the material heating. This phenomenon is called *blockage effect* and it is able to considerably reduce the inner temperature of the heat shield [7,10]. The flux of pyrolysis gasses throughout the material can only be effective if the structure has mainly open porosities [11]. In fact, gas heating

* Corresponding author.
E-mail address: laura.paglia@uniroma1.it (L. Paglia).

https://doi.org/10.1016/j.matdes.2024.113014
Received 8 February 2024; Received in revised form 1 May 2024; Accepted 10 May 2024
Available online 11 May 2024

within closed porosities can lead to uncontrolled pressure increase, thus causing crack formation and spallation of the material. For this reason, carbon-phenolic ablators need to be produced following a manufacturing strategy able to guarantee homogeneity, low density, low thermal conductivity and open porosity. In recent studies by E. Poloni et al. [12–15] polyvinylpyrrolidone was added to a standard carbon-phenolic ablator in order to modify and control its microstructure and porosity. Yin et al. [16] worked at a novel low density ablative material with a resin/silicone hybrid aerogel as matrix obtaining an ablator with hierarchically micro-*meso*-macro porous structure and proved its higher thermal stability. Other researchers obtained successful results in controlling the porous structure of light-weight ablative materials by a sol–gel process with the addition of organic compounds [17,18]. Thus, additives and fillers can influence the microstructure of the resin with possible beneficial effects in terms of thermal conductivity reduction [11,18]. However, a polymeric additive can participate in the chemical decomposition of the matrix modifying the amount of heat absorbed during the endothermic reaction [19]. The polymeric additive may or may not form chemical bonds with the chains of the phenolic resin during its polymerization: in the first case, these bonds break during the decomposition, with further energy consumption; in the second case, a blend is formed and the two polymers decompose absorbing energy according to their specific nature [20]. The addition of additives in the carbon-phenolic ablators need to be deeply investigated in order to understand how their physical and chemical properties can influence the overall material performance, but this kind of analysis was not found in the present literature, to the knowledge of the authors. Thus, with the purpose of providing new useful information, in the presented research work, standard and PVP-enriched ablators with a density of about 0.3 g/cm^3 were manufactured and the chemical interaction between phenolic resin and PVP were investigated through infrared spectrometry (FTIR). The microstructure of standard and PVP-enriched ablators was observed with a scanning electron microscope (SEM) and, for selected samples, a X-ray Microscopy (XRM) analysis was carried out for studying the porosity and the distribution of the resin inside the samples [21]. In order to assess the influence of PVP addition on the mechanical properties of a carbon-phenolic ablative material, compression tests were carried out on standard and PVP-enriched ablators, both in virgin and charred state. At last, ablative performance were evaluated with oxyacetylene flame exposure tests. This research activity provides important information about the potentialities of PVP-enriched ablators, in particular giving an interesting insight in how the microstructure can be modified and analyzing the chemical and physical phenomena connected with PVP addition in carbon-phenolic composites.

2. Materials and methods

2.1. Raw materials and manufacturing strategy

A commercial resole phenolic resin (Cellobond SC1008P, Hexion chemicals) was selected as matrix material because of its high oxidation resistance, low viscosity (about 250 cP at T = 25 °C), elevated heat of ablation, and a char yield of 55–60 % at temperatures above 650 °C [22]. A rigid graphitic felt (Sigratherm MFA, SGL Carbon SE, Germany) was selected as reinforcement material to be impregnated by the phenolic resin. Sigratherm MFA is a shape retentive insulating material, made of randomly distributed carbon fibers connected by a carbonaceous binder, residual from the pyrolysis of a phenolic resin [1]. Ethylene glycol was selected as solvent for the uncured phenolic resin because it promotes the formation of a gel phase during the curing process of the phenolic resin and it facilitates the formation of open and interconnected pores [13], thus ensuring a homogeneous resin distribution within the carbon felt [23]. Polyvinylpyrrolidone (Thermo Scientific™) was used as polymeric additive, as explained in the previous section. Carbon-phenolic ablators were manufactured by infiltrating cylindrical-shaped graphitic felts with a solution of phenolic resin, ethylene glycol and polyvinylpyrrolidone (PVP). Firstly, the manufacturing process has been optimized to guarantee a good distribution of the phenolic resin inside the carbon felt and to control the phase separation process during the gel formation in the curing phase: this step is essential for obtaining a micro and nanostructured resin distributed among the carbon fibers. Once the process was defined, samples with different resin/solvent ratio and percentage of PVP were prepared, as displayed in Table 1. Samples without the addition of PVP were prepared too and used as reference materials. The resin-to-solvent ratio was varied in order to obtain a final density of 0.32 ± 0.03 g/cm^3, while the PVP percentage was set with respect to the resin weight, in order to investigate the effects of different amount of PVP addition on the final structure of the resin.

The manufacturing process was designed on the basis of well-established production procedures reported in previous works [18,23] and considering the issues related to the PVP addition [13]. Thus, PVP was dissolved in ethylene glycol using an ultrasonic and heating bath (Elmasonic S30H); the phenolic resin was dissolved in ethylene glycol too using a hot plate and magnetic stirring. The solutions were merged once the temperature of 110 °C was reached. The carbon felts were then inserted in the solution, stirred and heated to 150 °C and maintained at this temperature until the formation of the gel phase began to take place. It is possible to recognize the incipient gel formation because of a change in the color of the solution: before it is clear and then it turns opaque/turbid because the molecular chain network starts to form [23]. Once the incipience of the gel formation was observed, the samples were transferred inside an oven, while still immersed in the solution, and kept at 150 °C for 12 h. Thereafter, the excess of gel was removed, and the samples were put back in the oven for the final curing steps: 160 °C for 8 h, 170 °C for 8 h and 180 °C for 8 h. The composition and the nomenclature of the manufactured ablators is reported in Table 1. Two different resin-to-solvent ratios were selected: during the process optimization also ratios of 240 and 500 g/l were attempted, but in those cases the final density of the ablators was too high compared with the target density of about 0.3 g/cm3. PVP was added in three different percentage with respect to the mass of the uncured resin. Thus the samples were named *x/y* where *x* is the resin concentration in the initial solution of resin and ethylene glycol (160 or 200 g/l) and *y* is the PVP weight percentage (0, 5, 10 or 20 wt%).

2.2. Infrared spectroscopy

FTIR spectra were acquired by a Bruker Vertex 70 spectrophotometer in Attenuated Total Reflectance (ATR) mode with a resolution of 4 nm^{-1}, 32 scans, over a spectral range of 4000–600 cm^{-1}. Spectra were recorded on ground powder samples and deposited on the sample holder as a solid matrix or as a thin film from ethanol (EtOH) in the case of PVP.

2.3. X-ray microscopy (XRM)

X-ray microscopy is a nondestructive technique of analysis able to create images of the internal features of the examined samples, thanks to the difference in absorption of X-rays by the different materials components and phases. XRM has been widely used in energy materials research [24,25], additive manufacturing [26], cultural heritage [27,28] and life sciences [29,30]. The experimental setup for XRM analysis is typically composed of three main elements: (i) the source

Table 1
Composition and nomenclature for manufactured samples.

Phenolic resin and ethylene glycol ratio	Percentage of PVP with respect to the phenolic resin weight			
	0 %	5 %	10 %	20 %
160 g/l	160/0	160/5	160/10	160/20
200 g/l	200/0	200/5	200/10	200/20

where the X-ray beam formation occurs, (ii) the sample stage that firmly holds the sample in the desired position and ensures its rotation during the experiment and (iii) the detector, which is a charge-coupled device (CCD) or a complementary metal-oxide semiconductor (CMOS), that collects the transmitted X-ray beam. XRM principle is based on the X-ray computed tomography (CT) approach to collect 3D images of specimen internal features. This is achieved by acquiring a set of 2D projections at different scan angles while rotating the sample and exposing it to the X-ray beam. In this study XRM scans were performed using a ZEISS Xradia Versa 610 X-ray microscope equipped with a 0.4x objective lens to provide a 3D isotropic voxel size of 17 μm across the imaging volume. Each Volume of Interest (VOI) was scanned setting a source voltage and power of 40 kV and 3 W respectively, camera Bin 2, 5.00 s exposure time and 1601 projections. No source filter was required. The resulting projection images, i.e. radiographies, were reconstructed using the Reconstructor Scout-and-Scan (V. 15.0.17350) software and thea Feldkamp-Davis-Kress (FDK) algorithm [31] Samples were investigated along the vertical axis to cover the entire length of the objects. The resulting datasets from each sample were then stitched together producing a 3D volume covering every specimen in its entirety. XRM datasets were filtered using a Non-Local Means filter (Kernel Size 7; Smoothing 0.5) and analyzed using Dragonfly Pro from Object Research Systems (ORS).

2.4. Compression tests

Compression tests were performed on standard and PVP-enriched ablators for a selected resin-to-solvent ratio and percentage of PVP addition: samples 200/0 and 200/10 were cut in cylinders with an height of 30 mm and a diameter of 15 mm. The tests were carried out according to the procedure proposed by Parmenter et al. [32] for the mechanical characterization of PICA and considering also the ASTM standard C165-07 [33].Three samples for each kind of material were tested both in virgin and charred state. The ablators were charred in a tube furnace (Carbolite Gero, TF1-1600) equipped with a dense alumina tube under an inert atmosphere of nitrogen with a flux of 5 Nl/min. The chamber was heated up from room temperature to 1000 °C with a heating rate of 5 °C/min. The maximum temperature was kept constant for 1 h and then the furnace was cooled down slowly to avoid damaging. Compression tests were performed with a Zwick Roell Z010 mechanical testing machine equipped with a 10kN load cell and the tests were performed with a crosshead speed of 10 mm/min.

2.5. Oxyacetylene torch test

The oxyacetylene torch test is designed for determining the performances of ablative materials in terms of insulation effectiveness and recession rate in order to identify the more promising formulations. The exposure tests were carried out according to the ASTM standard E 285–08 [34] with a fully-automated and controlled facility designed and engineered by the Laboratory of Materials and Surface Engineering of Sapienza University of Rome [1,8,9,23,35,36]. Fig. 1 shows the scheme and a picture of the facility during an on-going test.

As described in previous works [1,8,9,23,35,36]. An oxyacetylene flame was obtained with the combustion of the oxygen and acetylene. The ratio between the fuel and the oxidizer determines if the obtained flame is oxidizing, neutral or reducing. The ASTM standard [34] recommends a neutral/reducing condition in order to test ablative materials without causing oxidation. For this reason, tests were carried out with the flow rate set at 315 Nl/h for acetylene and 300 Nl/h for oxygen. During the test it is necessary to guarantee a known and constant heat flux that is calibrated by a cold wall heat flux sensor (HFM 1000 Vatell Corporation, Christiansburg, Virginia USA), while surface and back temperature of the tested samples are measured respectively with a two-color digital pyrometer (Impac Infrared, Frankfurt, Germany) and a k-thermocouple put inside the specimen at a known distance from the exposed surface. Surface and back temperatures are acquired during the oxyacetylene flame exposure by a data acquisition system (National Instrumentand) and input and output parameters are managed by a LabView software. Samples of Sapienza Ablative Material were tested for 60 s with a cold wall heat flux set at 4 MW/m^2. After 60 s of exposure the samples were quickly cooled down with a flux of CO_2 in order to limit possible post-test oxidation phenomena induced by the slow cooling down in air. Weight and dimensions of each specimen were collected before and after the test in order to evaluate the weight loss and the surface recession.

3. Results and discussion

3.1. Manufacturing optimization

The manufacturing optimization was carried out to investigate the influence of parameters such as time, temperature and PVP content on the final microstructure of the resin and on its homogeneous distribution within the carbon felt. The performance of a carbon-phenolic ablator is strictly connected with its microstructure: open porosities and a meso/nano-structure of the phenolic resin can enhance the thermal

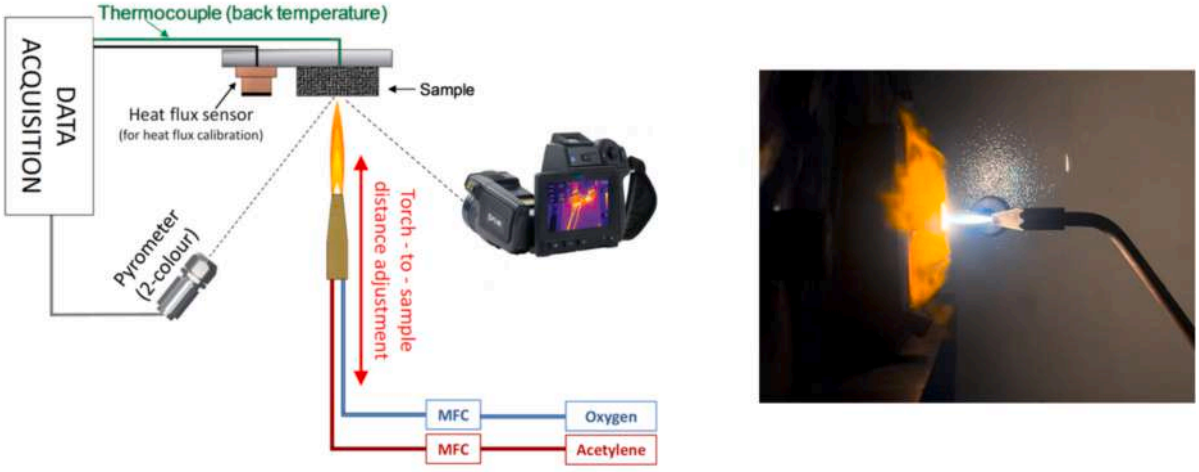

Fig. 1. Oxyacetyelne flame burner scheme (on the left) and picture (on the right).

insulation properties and can guarantee low density and an optimized resin distribution [16,37,38]. According to Yin et al. [16] aerogels characterized by micro/nano-porosities are promising thermal protection materials in high temperature environment for many space applications thanks to their low thermal conductivity. Furthermore Noparvar et al [38] assess that the high void percentage of aerogel combined with a peculiar porosity at the micro/nano-scale allowed for obtaining low mass density and an extremely low thermal conductivity which are very desired properties for space applications. Saliman et al. [39] specified that the physical properties of porous materials depends on the kind, shape, and size of the pores and their peculiarities are a result of the special arrangement of their network structure. A strategy for obtaining such result is to allow the formation of an aerogel with phenolic resin precursors, a solvent and the addition of some organic additives [37]. In this way, with a proper curing, the phenolic resin passes through a gel phase where two different kinds of domains form: one with a higher resin concentration and another with an higher solvent amount [16]. When the cure proceeds, the solvent is removed by heating and the solid resin has a microstructure with characteristic open porosities. In this process the dimension of the domains during the gelation and, as a consequence, the dimension of the open porosities of the cured resin, can be influenced by the organic additive [16]. In this research numerous attempts were carried out to obtain PVP-enriched carbon phenolic ablators with an aerogel-like microstructure of the phenolic resin. In particular we paid attention to the gel-forming temperature, to the impregnation time and temperature and to the final step of cure in the oven. The optimized temperature for gel-forming step was found to be 150 °C: the development of a gel phase at lower temperatures has resulted in an uneven structure within the felt, while the formation of the gel at temperatures higher than 150 °C has led to a too fast formation of the polymer networks thus preventing the development of a microstructured resin. As a first attempt the carbon felt samples were submerged inside the solution at 150 °C on the hot plate with a vigorous stirring and the temperature were gradually increased until the gel formation. Then the samples were removed from the gel and cured in the oven at 180 °C. Even if this procedure influences the microstructure of the resin and promotes the formation of a micrometric globular microstructure it was not satisfactory because the resin was distributed only on the carbon felt and it was not uniform. Thus, after the solution heating at 150 °C on the hot plate, the samples (still submerged in the solution) were put inside an oven at 150 °C. In this way, after some hours, the gel forms. The consistence of the gel was periodically controlled and, after 12 h the gel was well formed and it was still easy to remove the samples from the gelified solution. Thus it was established a curing step in oven at 150 °C for 12 h. After this step the samples were removed from the gel and put in the oven at 180 °C for 24 h, but this procedure leaded to and over-curing of the resin, thus the temperature was gradually increased and the samples were cured at 160 °C for 8 h, 170 °C for 8 h and 180 °C for 8 h with a more satisfactory result.

Following the aforementioned procedure, several samples were manufactured with different resin/solvent ratio and PVP content (Table 1) and their mean densities were reassumed in Table 2. Microstructural analysis performed through SEM revealed that the microstructure is mostly influenced by the amount of PVP inserted in the solution: Fig. 2 and Fig. 3 show the SE micrographs of the samples with a resin/solvent ratio of 160 g/l and 200 g/l respectively and different PVP percentages. Compared to the reference samples 160/0 and 200/0, in which the resin covers the fibers forming a smooth surface, all PVP-enriched samples are characterized by the formation of a granular-structured resin distributed all over the fibers: the 160/5, 200/5, 160/10 and 200/10 samples show a similar distribution of the resin above the carbon fibers, while in the 160/20 and 200/20 samples the resin forms an interconnected network between the fibers. Higher magnification micrographs show the nano-structured resin when PVP is added to the ablators (Fig. 2 (c,f,i,n), Fig. 3 (c,f,i,n)).

Table 2
Average densities of the manufactured samples.

PVP (%)	160 g/l	200 g/l
0	0.324 ± 0.020 g/cm^3	0.316 ± 0.005 g/cm^3
5	0.316 ± 0.014 g/cm^3	0.323 ± 0.005 g/cm^3
10	0.302 ± 0.021 g/cm^3	0.322 ± 0.014 g/cm^3
20	0.334 ± 0.018 g/cm^3	0.356 ± 0.010 g/cm^3

3.2. FTIR results

The characterization of chemical structure was performed via infrared spectroscopy in ATR mode on PVP and phenolic resin (PhR) precursors and in blended (PVP-phenolic) cured samples. The blended samples analyzed by FTIR were produced without carbon felt, so that the resin/ PVP samples were reduced to powder and made suitable for the FTIR analysis. These samples were named PhR + PVP5%, PhR + PVP10%, PhR + PVP20% according to the content of PVP in weight percent. According to literature [40,41], for PVP sample (Fig. 4a, red line), the broad band at 3381 cm^{-1} corresponds to the adsorbed water, which most probably originated from pure polyvinylpyrrolidone (PVP) interaction with moisture. Asymmetric stretching (ν) vibrations of –CH2- of pyrrolidone ring appear at 2966 cm^{-1}, whereas aliphatic methylene chains show asymmetric and symmetric ν(–CH2-) at 2925 cm^{-1}, 2876 cm^{-1}, respectively. Peculiar stretching vibration of C = O of amide functional group at solid state can be found at 1656 cm^{-1} with corresponding ν(C–N) centered at 1288 cm^{-1} (pyrrolidone ring). Aliphatic ν(C–N) give rise to an absorption band at 1174 cm^{-1}. Further deformation vibrations, i.e., scissoring, bending, and wagging, arising from both cyclic and aliphatic methylene chains appear in the 1494–650 cm^{-1} wavenumber region. Complete PVP FTIR bands assignment is reported in Table S1.

Cured phenolic resole resin (Fig. 4b, black line) shows a broad absorption at around 3285 cm^{-1} as typical stretching vibration of –OH groups, partially overlapped with aromatic ν(C–H) in the 3000–3100 cm^{-1} range. Aliphatic ν(–CH2-) vibrations can be found at 2932 cm^{-1} (asymmetric) and 2880 cm^{-1} (symmetric). Medium intense bands due to ν(−C = C-) and aromatic skeletal deformation vibrations are at 1606 cm^{-1} and 1511 cm^{-1}, respectively, can also be observed. In-plane ν(−O–H) phenolic and ν(=C–OH) vibrations give rise to absorptions in the 1360–1200 cm^{-1} wavenumber region, whereas single bond ν(−C–OH) is at 1143 cm^{-1}. Symmetrical (C–O–C) stretching of aliphatic chain can be found at 1037 cm^{-1}. Typical out-of-plane deformation vibrations of trisubstituted benzene rings appear in the 880–656 cm^{-1} range. According to literature [42], complete FTIR bands assignment of cured phenolic resin is reported in Table S2.

FTIR-ATR spectroscopy allows to identify characteristic PVP and PhR functional groups in ablative blended samples taking pristine precursors as reference materials (Fig. 4a). Focusing on the 1800–600 cm^{-1} wavenumber region, the FTIR spectrum of PhR + PVP 5 % (Fig. 4b, orange line) shows the typical stretching vibration of C = O of PVP amide group centered at 1654 cm^{-1} and a shoulder at 1511 cm^{-1} indicative of the presence of aromatic PhR counterpart. Differences between PVP, cured PhR and PhR + PVP 5 % can be observed in the 1500–1450 cm^{-1} wavenumber region. Indeed, bands at 1462 cm^{-1} (PVP, –CH2 scissoring), 1475 cm^{-1} and 1440 cm^{-1} (PhR, –CH2- bending of methylene bridge and in-plane –CH2- scissoring, respectively) give rise to a broader absorption with little-to-no wavenumber shift.

A combination of –CH2- wagging of PVP aliphatic chain at 1288 cm^{-1}, 1271 cm^{-1} and ν(=C–OH) at 1211 cm^{-1} arises in the 1300–1270 cm^{-1} range. Spectra of PhR + PVP 10 % (Fig. 4b, brown line) and PhR + PVP 20 % (Fig. 4b, red line) show common absorptions with significant differences from those observed in pristine ablative precursors. Specifically, the appearance of 1653 cm^{-1} and 1601 cm^{-1} bands associated with ν(C = O) of PVP amide group and ν(−C = C-) of PhR aromatic ring, respectively, confirmed the presence of both PVP and PhR in the final

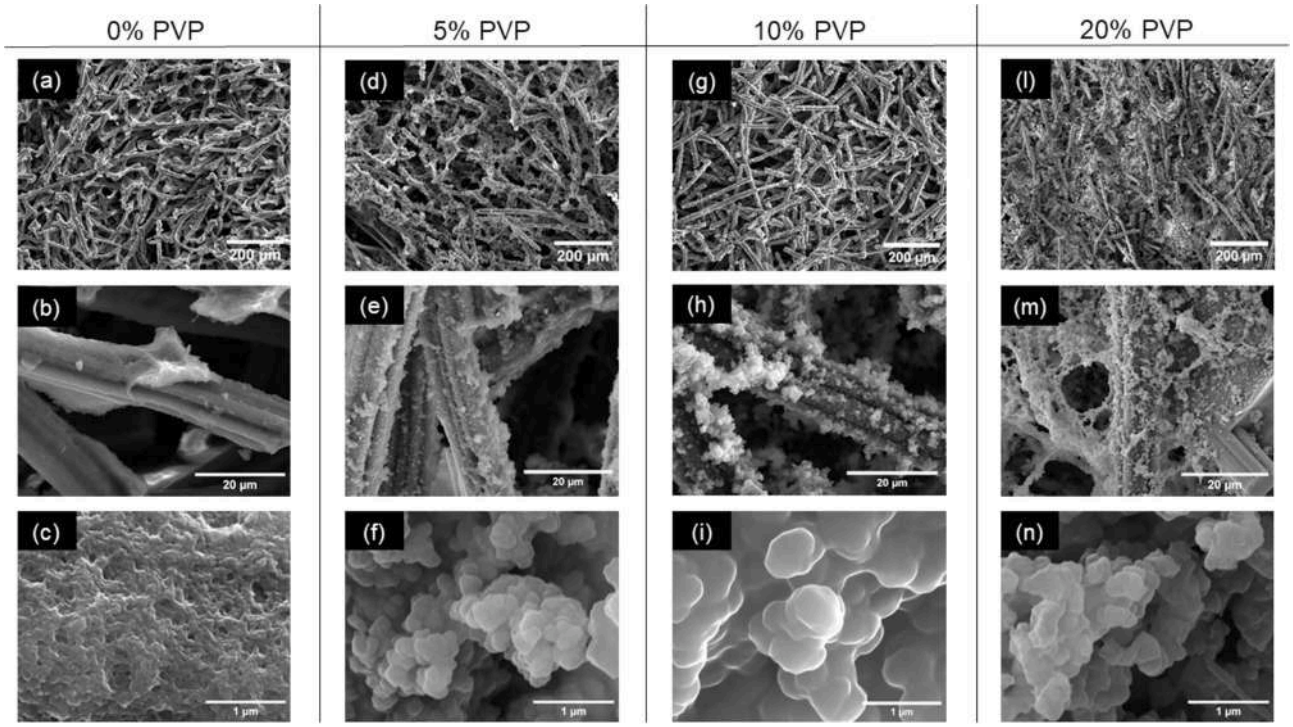

Fig. 2. SE micrographs at different magnifications for 160/0 (a,b,c), 160/5 (d,e,f), 160/10 (g,h,i), 160/20 (l,m,n).

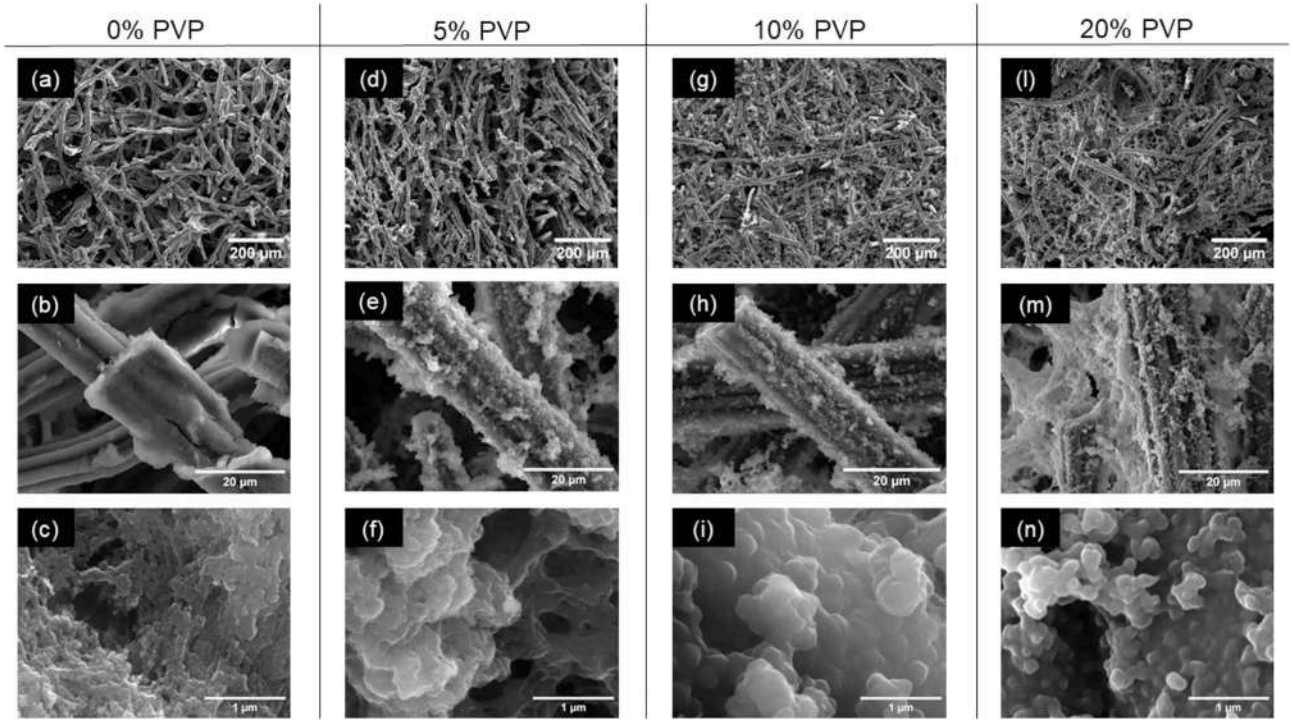

Fig. 3. SE micrographs at different magnifications for 200/0 (a,b,c), 200/5 (d,e,f), 200/10 (g,h,i), 200/20 (l,m,n).

products. When the concentration of PVP in the ablative samples is higher, the bands in the 1460–1440 cm^{-1} region (1462, 1442 cm^{-1}) associated with –CH2- scissoring vibration widen. Changes can also be observed in the relative intensity of bands at 1270 cm^{-1} and 1210 cm^{-1} due to aliphatic –CH2- deformation vibration (wagging) and ν(=C–OH) of PhR. The vibrational bands at about 1080 cm^{-1} (C–H stretching vibrations of aromatic ring and C–C skeletal vibrations) and at 1030 cm^{-1} associated with ν(C–O–C) and C–C, C–H deformation modes disappeared in both PhR + PVP 10 % and PhR + PVP 20 % samples. A similar behavior was observed for bands centered at 876 cm^{-1} and 825 cm^{-1} associated with out-of-plane deformation mode of aromatic rings of PhR and can be considered as a sign of π-π stacking interactions between PhR chains. Since no band shifts in all FTIR spectra was detected, it can be stated that blended ablative material are mainly characterized by

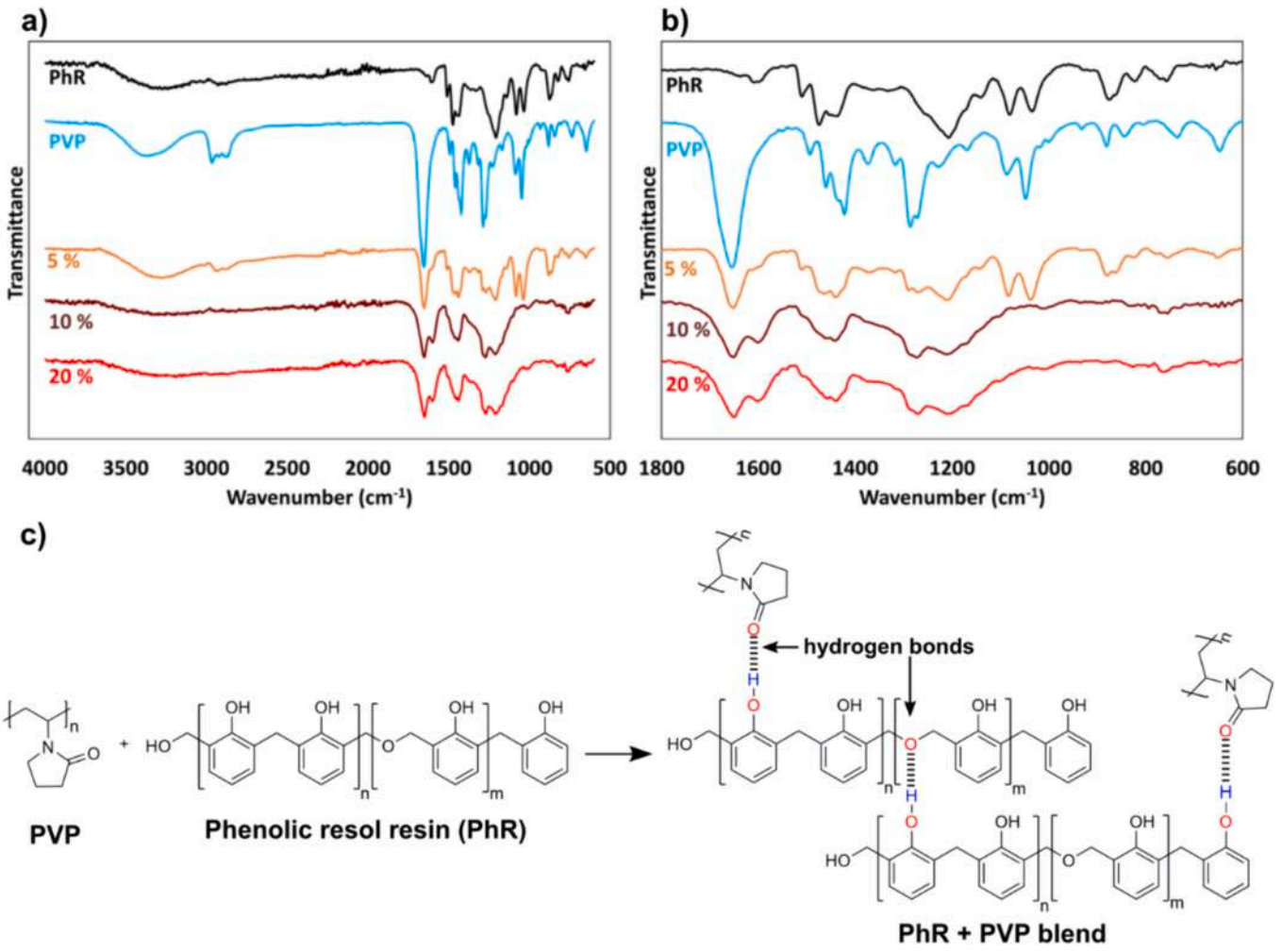

Fig. 4. A) ftir-atr spectrum in the range of 4000–600 cm^{-1} of pure polyvinylpyrrolidone (PVP); cured phenolic resin (PhR, powder); phenolic resin with 5 wt% of PVP (5 wt%, ground powder); phenolic resin with 10 wt% of PVP (10 wt%, ground powder); phenolic resin with 20 wt% of PVP (20 %, ground powder); b) FTIR-ATR spectrum in the 1800–600 cm^{-1} wavenumber region; c) Schematic representation of the interactions occurring in PhR + PVP blends.

physical non-covalent interactions between PVP and phenolic resin; moreover disappearance or changes in the intensities of most bands indicate high miscibility in PVP/PhR system [43] with hydrogen bonds contribution [44]. Specifically, the presence of heteroatoms on both PVP and PhR structure led to hydrogen bond formation in which phenolic hydroxyl group, ether PhR functional group and carbonyl group (C = O amide) in the pyrrolidone ring are responsible for hydrogen bond formation and hydrophobic effects which improve the physical/mechanical properties of the blends. In detail, PhR possess –OH directly bonded to the aromatic ring (phenols) which can act as both hydrogen bond donor and acceptor, whereas the ether C–O–C groups of PhR (1047 cm^{-1}) and the C = O of cyclic amide (ca. 1650 cm^{-1}) can act both as H-bond acceptors. Thus, the decrease in intensities of bands around 3200 cm^{-1} (ν(−O–H)), 1210 cm^{-1} (ν(=C–OH)), and 1145 cm^{-1} (single bond ν(−C–OH)) suggests the involvement of hydroxyl groups in weak (noncovalent) intermolecular interactions, which are more pronounced passing from phenolic resin with 5 wt% of PVP to phenolic resin with 20 wt% of PVP. A decrease in the intensity occurs also in the band at 1047 cm^{-1}, due to ν(C–O–C). Changes in the band at 1084 cm^{-1} due to C–H stretching vibrations of aromatic ring and C–C skeletal vibrations are also observable, corroborating the possible π-π stacking interactions between PhR chains. After blending, a change in the relative intensities of ν(C = O) bands of PVP amide group at ca. 1650 cm^{-1} occurs for phenolic resin with 10 wt% and 15 wt% of PVP, which can be assigned to free (1653 cm^{-1}) and H bonded C = O units (1600 cm^{-1}) [45]. The presence of donor and acceptor groups in the polymeric chains and the variations occurring in the spectra agree with the formation of inter-chain interactions among PhR and PVP in form of hydrogen bonds as reported for similar blend formulations (Fig. 4c). [46–48]. It is worthy to note that hydrogen bonds can also take place between PhR, stabilizing the structure of the composite materials. Complete FTIR bands [49] assignments of ablative samples are reported in Table S3-S5.

3.3. Mechanical test results

The mechanical test results were reassumed in Fig. 5, in particular Fig. 5 (a) shows rapresentative stress–strain curves for ech kind of tested sample, while in Fig. 5 (b) an instogram compares the maximum stresses recorded during the test. The virgin samples behave differently if the ablator is enriched or not with PVP: the average values of maximum stress is higher when the PVP is added to the material, even if the standard deviation is quite high and this difference is not so relevant. A substantial difference is observed for the mechanical behavior of the charred samples: when PVP is added to the ablator, the charred samples show higher mechanical performance. Furthermore the drop of mechanical performance between the virgin and the charred state is lower with PVP: for standard ablator, this drop is about 64 %, whereas for PVP it is reduced to 20 %. The polyvinylpyrrolidone has lower mechanical properties compared with the phenolic resin [50,51] and it decomposes totally when exposed to temperature higher than 600 °C both in inert

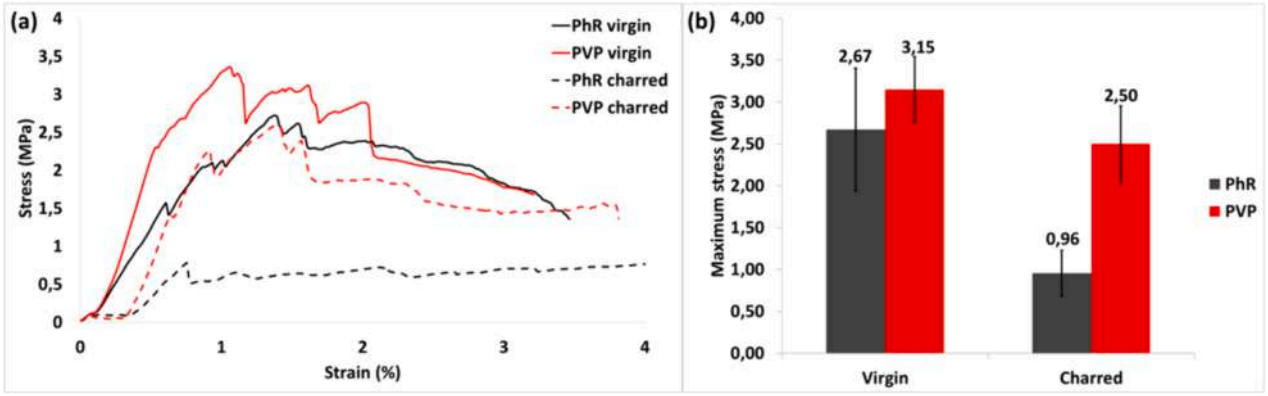

Fig. 5. (a) Representative stress–strain curves for compression tests on virgin and charred samples; (b) Maximum stress for virgin and charred samples.

and oxidizing atmosphere [52] and so it is no more present in the charred samples. Thus, the important improvement is totally due to the different distribution of the phenolic resin inside the samples.

3.4. Oxyacetylene flame exposure results

During oxyacetylene torch tests the back temperature was recorded with a k-thermocouple set inside the sample at 2 cm from the exposed surface while a two-color pyrometer recorded the temperature of the exposed surface. Three samples for each kind of material were tested in the same condition at 4 MW/m^2 for 60 s. The surface temperature results are summarized in Fig. 6: representative curves are selected in order to more easily distinguish the different behaviors of the ablators, while the average surface temperature recorded after 55 s of exposure are reported in the histogram.

From these results it is evident that both the resin concentration and the percentage of PVP can influence the samples thermal behavior: the higher the PVP content, the higher the surface temperature for the ablators manufactured with a resin concentration of 160 g/l, whereas for samples manufactured with a resin concentration of 200 g/l the surface temperature is minimum for 200/10 specimens. Samples 160/0, 200/0, 160/5 and 200/5 show that the surface temperature is strongly influenced by resin/solvent ratio in case of specimens with the lower PVP content (5 wt%). In fact, for each resin/solvent ratio the difference in surface temperature between samples with 0 or 5 wt% of PVP is negligible. Thus it is possible to asses that for ablators with 0 and 5 wt% of PVP the surface temperature is more influenced by the resin to solvent ratio, while for ablators with higher PVP content (10 or 20 wt%) the surface temperature is more influenced by the amount of PVP. More specifically, samples with 20 wt% of PVP exhibit the highest surface temperature at the end of the exposure test.

The back temperature data collected during the torch tests are reported in Fig. 7; the samples without the addition of PVP (160/0 and 200/0) show the worst thermal performance: after a plateau, the temperature starts to rise and it keeps always higher than PVP enriched samples. The back temperature curves for samples with 5 and 10 % of PVP are very similar, both in trends and in the value after 55 s of exposure, while the samples 160/20 and 200/20 show a slightly different behavior: the temperature starts to rise after about 10 s of exposure, that is a much longer time if compared to the other samples (~3 s). Fig. 7c, showing the back temperatures after 55 s, seems to indicate that the PVP addition has a strong impact on the ablator thermal performance. The mass loss and the surface recession were also evaluated to better understand the ablation phenomena (Fig. 8). The mass loss is very similar for all the tested ablators and the observed mass loss trend follows values of samples density (Table 2): the higher the material density, the higher the mass loss due to the greater amount of resin and PVP, which decompose producing gas species. The production of outgassing pyrolysis gases is an effective mechanism of heat dissipation [9,53,54], but it also provides an important contribution to mass loss. The surface recession results are strongly influenced both by the PVP content and by the resin to solvent ratio: the most intense surface recession is reached for samples modified by 20 % wt. of PVP; nevertheless, the ablators manufactured with a resin concentration of 160 g/l exhibit a surface recession that is always lower than samples with a resin content of 200 g/l for each amount of PVP addition (5, 10 and 20 % wt.).

The SEM micrographs of the samples exposed surface after the torch tests are shown in Fig. 9: it is possible to observe the different morphology of the char residue and how it is distributed on the carbon fibers. Standard samples (160/0, Fig. 9a and 200/0, Fig. 9e) show a porous char and oxidized carbon fibers, while samples modified by 5 and 10 % wt. of PVP (Fig. 9b, c, f, g), show a carbonaceous residue with a morphology similar to the virgin (not pyrolyzed) resin and fibers less oxidized and well covered by a char layer. In the ablator 160/20

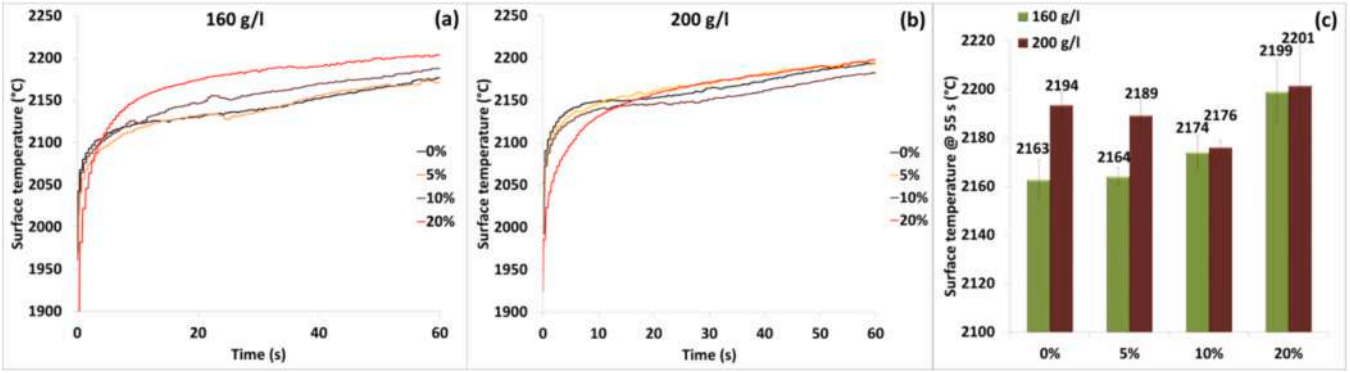

Fig. 6. Graphs with the trend of surface temperature during the oxyacetylene torch test (a,b) and histogram (c) with average values of temperature at 55 s.

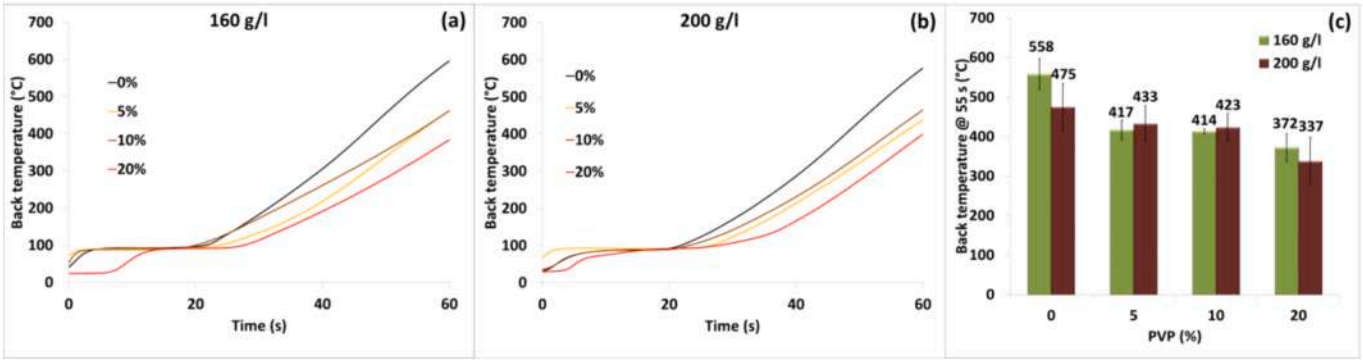

Fig. 7. Graphs (a,b) with the back temperature trend during the oxyacetylene torch test and histogram (c) with the average values of temperature after 55 s of exposure.

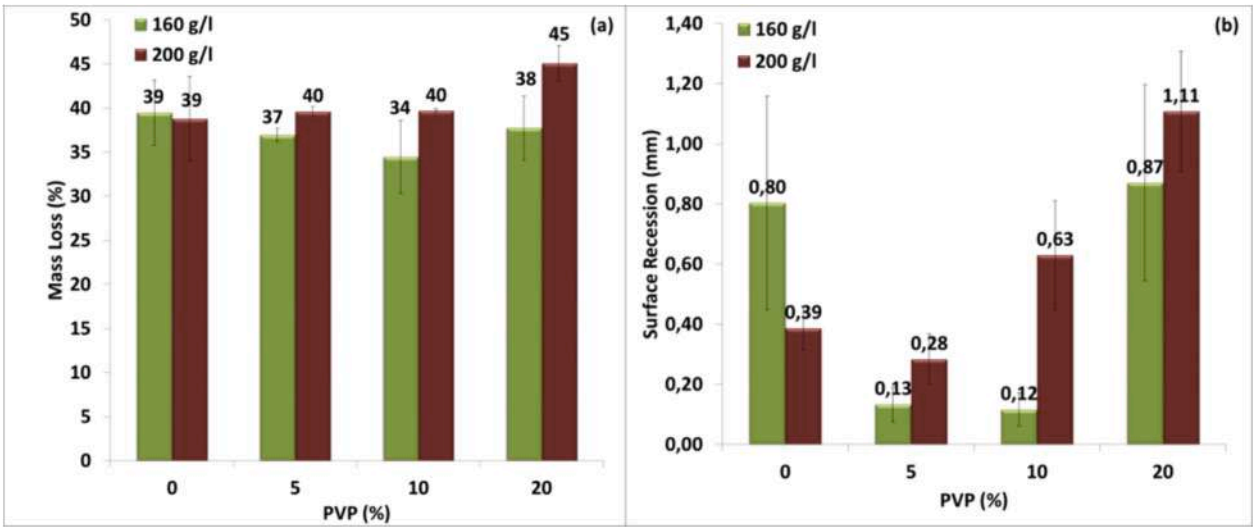

Fig.8. Mass loss (a) and surface recession (b) for samples tested with the oxyacetylene torch.

(Fig. 9d) the carbonaceous residue is very porous and it is distributed not only on the fibers surface but also among them. The exposed surface of the ablator 200/20 shows areas with different morphologies: the first one (Fig. 9 h) is characterized by oxidized fibers and a porous carbonaceous residue, whereas the other one (Fig. 9 i) is completely covered with a dense charred layer having globular morphology. The exposed samples were cut along their main axis in order to observe their cross section: as an example Fig. 10 shows the difference in sample 200/10 between the exposed surface (Fig. 10b) and the underlying material (Fig. 10c). This difference can be attributed to a shielding effect due to the outgassing: pyrolysis gases generated by the thermal decomposition of PVP and phenolic resin flow throughout the boundary layer hindering convective exchange, as already reported in several works [16,54]. This phenomenon causes a steep temperature gradient between the exposed surface and the inner part of the sample and so also a variation in the morphology.

The PVP addition can modify the ablative performance in different ways: firstly, as demonstrated by the SEM micrographs (Fig. 2 and Fig. 3), PVP can influence the microstructure of the carbon-phenolic ablator and the different microstructures have an influence on the thermal diffusivity of the material. In fact the samples with 20 wt% PVP show a more uniform resin distribution, not only on the carbon fibers, but also among them: the resulting highly micro/nano-porous structure is able to limit the thermal conductivity when a surface is exposed to a heat flux [18]. On the other hand, according to literature data [51] PVP, both in inert and oxidizing atmosphere, decomposes completely at 600 °C with almost only volatile products. As a consequence, when PVP-enriched ablators are exposed to an heat flux, an overall increase of mass loss and a decrease in char yield is expected compared with the standard ablators. Thus, as demonstrated by the oxyacetylene torch test, the addition of PVP is beneficial for the thermal performance of the ablator (lower back temperature), but it can decrease the mechanical properties of the char residue with consequent higher mass loss and surface recession. This aspect is disadvantageous because a high char yield of the ablative shield is essential for withstanding the intense shear stress typical of the atmospheric reentry [8,55]. Thus, PVP influences the overall char yield, and the carbonaceous residue can be more brittle and more easily removed. PVP addition can also modify the overall amount of heat involved in the endothermic processes: according to FTIR analysis, PVP interacts with the phenolic resin by means of weak bonds that have to be broken during the decomposition, thus absorbing part of the incoming thermal energy. Moreover, PVP modifies the morphology of the cured resin, changing for example the porosity distribution, thus influencing the thermal conductivity: it is known that the porosities and the pore size have a huge impact on the insulation performance [56]. The presence of PVP leads to reduction of the overall char yield but at the same time, to the increase of gases flowing throughout the charred material, thus enhancing the thermal performance. This phenomenon can be connected to the different shape of back temperature curves in samples with 20 wt% of PVP: the temperature starts to rise after a longer time and the plateau, which characterizes all the curves, is longer, probably because of the higher amount of

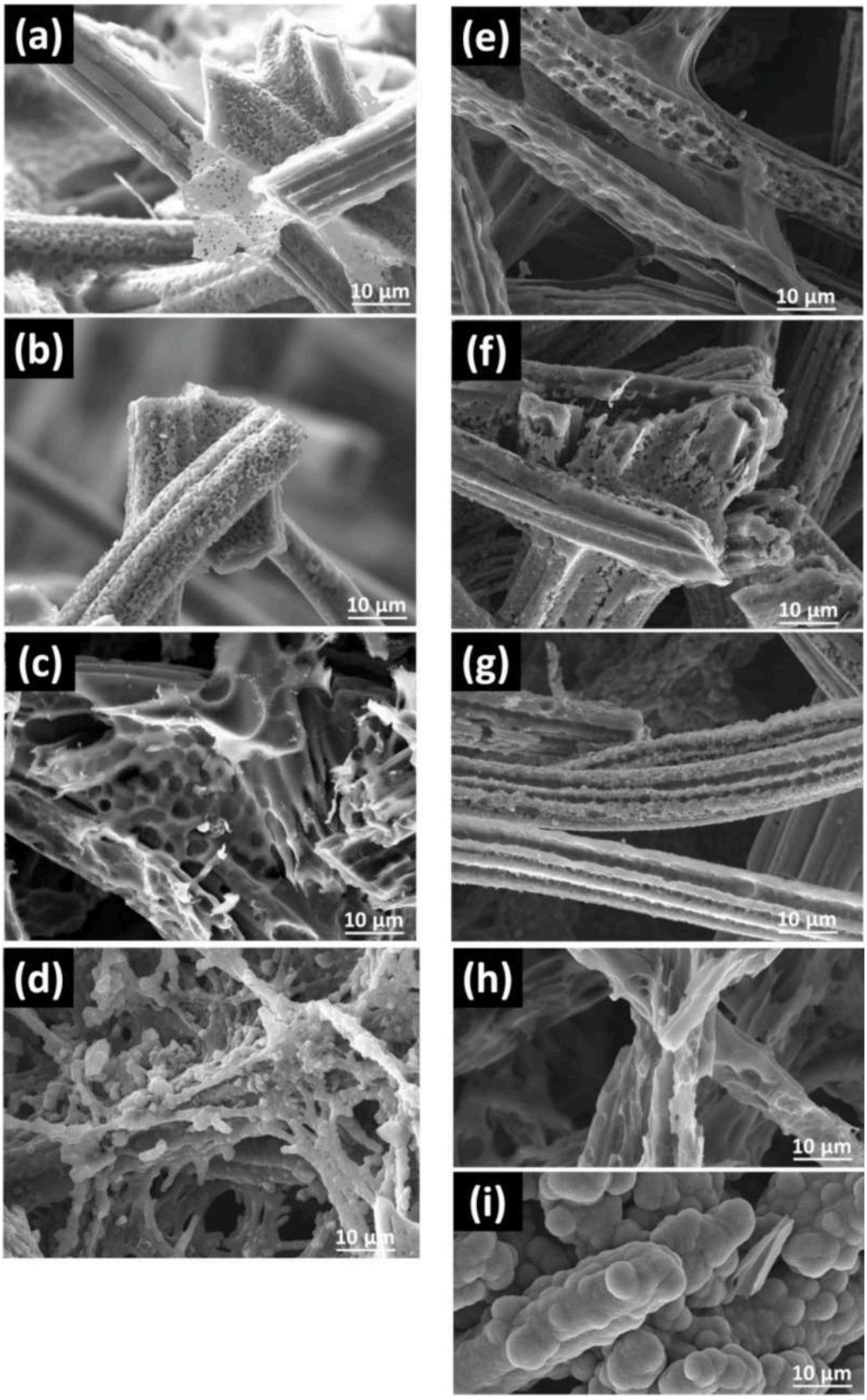

Fig. 9. SEM micrographs of the exposed surfaces after the oxyacetylene flame test (samples: 160/0 (a), 160/5 (b), 160/10 (c), 160/20 (d); 200/0 (e), 200/5 (f), 200/10 (g), 200/20 (h,i).

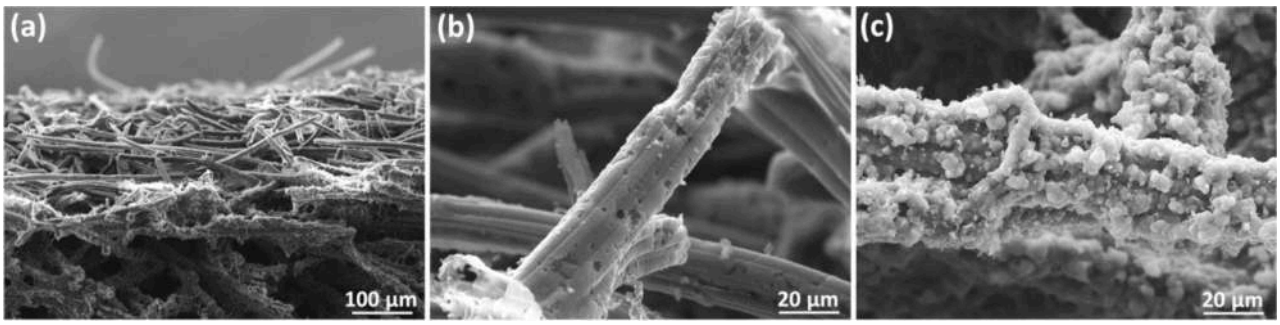

Fig. 10. SEM micrographs of sample 200/10 after the oxyacetylene torch test: a cross section near the exposed surface (a), fibers on the exposed surface (b), fibers just under the exposed surface (c).

outgassing decomposition products generated by the great quantity of added PVP. This behavior can also relate to the slower increase of surface temperature in samples 160/20 and 200/20. Poloni et al. [13] carried out a study on the effect of compounds addition to carbon-phenolic ablators and they correlate the dimension of the induced micro-porosities with the scattering of the thermal radiation at high temperature. Poloni assessed that the radiation scattering can be maximized when the dimension of the porosities is comparable with the wavelength corresponding to maximum black-body radiation. Thus, because of the different porosity and resin microstructure of samples with 20 wt% of PVP, the re-irradiation of the incident heat can be higher. This phenomenon can cause an increase in the surface temperature after a transient state and, at the same time, a decrease of the heat transmitted via thermal conduction [18].

3.5. XRM results

According to the data collected with FTIR and SEM analysis on virgin and charred ablators and according to the results of the oxyacetylene torch test, PVP-enriched carbon-phenolic ablators demonstrate enhanced ablative performance. While the sample 160/20 and 200/20 showed the best performance in terms of recorded back temperature, they also exhibit low char toughness, high surface recession rate and excessive mass loss. On the other hand the samples with 5 and 10 wt% of PVP show an improved thermal performance if compared to the standard ablators, with minimal recession and mass loss. For this reason, these composition (10 wt% of PVP) were selected for further characterizations using XRM analysis. Each sample was scanned and four cylindrical volumes, centered in the main axis of specimens, were analyzed. The technique allows for distinguishing voxels (volumetric picture elements) corresponding to high and low density according to the gray scale level. Three different main microstructures were identified and analyzed: (i) the first one with brighter voxels corresponds to phenolic resin agglomerates; (ii) the second volume, with darker voxels, corresponds to the macro-porosities; (iii) the third one refers to the zone with carbon fibers and the phenolic resin well dispersed among them. In this last sample portion, there are only micro-porosities and the corresponding voxels have an intermediate shade of gray. The results of this analysis are reported in Table 3: specimen 200/10 show the lowest resin agglomerates concentration and the highest percentage of macro-porosities. It is important also to correlate the XRM analysis results with the density of the analyzed samples. The two samples, 160/10B and 200/10B, selected for this analysis, show a density of 0.326 g/cm3 and 0.309 g/cm3 respectively and the volume without agglomerates or macro-porosities, is 84.78 % for 160/10 and 84.53 % for 200/10: the two samples are distinguished only for the agglomerates and voids. The sample 160/10 was analyzed by XRM both in the virgin and in the charred state, after the oxyacetylene flame exposure tests. For both samples, the images of seven 2D slices are reported in Fig. 11.

Table 3
XRM analysis results.

	Phenolic resin agglomerates (%vol)	Macro-porosities (%vol)
160/10	5.30 ± 0.36	9.92 ± 1.49
200/10	3.88 ± 0.78	11.59 ± 0.74

The slices are taken at a distance of 3.5 mm from each other, starting at 5 mm from the bottom. The slice A corresponds to the higher part of the sample and the slice naming proceeds sequentially until slice G near the bottom of the sample, as shown qualitatively in Fig. 11. At a first glance, the slice A in sample 160/10 virgin shows some big dark spots (macro-porosities) not present in the other ones, while slice D has an higher concentration of phenolic resin agglomerates observable as white areas. The other slices seems to be quite similar to each other and their non-homogeneities are mainly due to the fibers distribution in the MFA carbon felt. For the sample 160/10 char, the slices show the consequence of the oxyacetylene flame exposure. Slices F and G are pierced for the insertion of the thermocouple, but they are comparable to slice E. These slices are also similar to the sections of sample 160/10 virgin, but some darker sports can be noticed. A white circle, corresponding to a thin layer of phenolic resin, surrounding the carbon-phenolic cylindrical sample is present in slices E-G, but it almost completely disappears in slice D: this section is slightly different and it is evident that its edge was exposed to high temperature, causing a partial pyrolysis. The other three slices (A, B, C) are significantly different from the others and they show darker shades of grey. Indeed they show an area in which the high

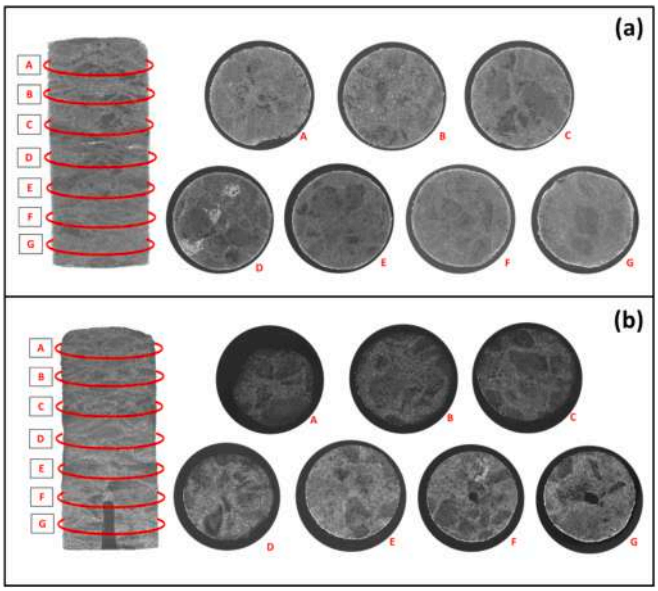

Fig. 11. XRM scan for virgin sample 160/10 (a) and charred sample 160/10(b).

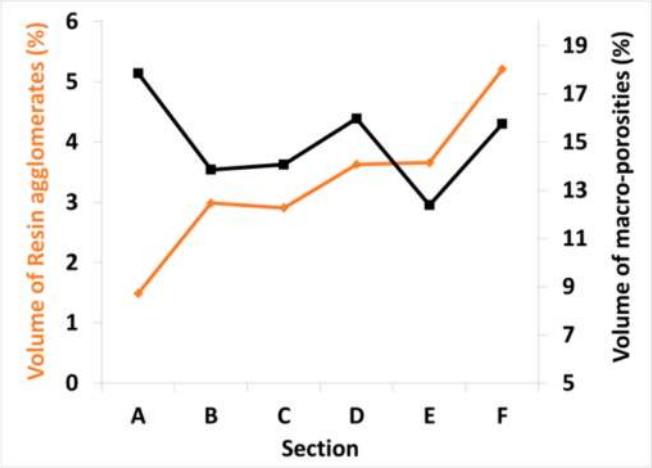

Fig. 12. Macro-porosities and resin agglomerates volume percentage in the charred sample 160/10.

temperature leaded to decomposition of phenolic resin and PVP and these areas mainly consist of carbon fibers and amorphous carbonaceous residue. Furthermore slice A has a smaller diameter due to the recession caused by the heat flux during the torch test. On the basis of the acquired data both the volume percentage of phenolic resin agglomerates and of macro-porosities were evaluated. The results are summarized in the graph of Fig. 12: the amount of phenolic resin agglomerates is lower in the section A near the exposed surface, and then it gradually increases reaching the maximum value of 5.21 % at the slice near the bottom. This value of resin agglomerates is comparable with the value of 5.30 ± 0.36 vol% found for the 160/10 virgin. The percentage of macro-porosities is higher in section A, near the exposed surface, and then, for the other sections, fluctuates around an average value of 14,41 vol%, higher than the value obtained for 160/10 virgin. Since the back temperature measured by the thermocouple reached 423 °C it is probable that the pyrolysis reaction began also at the bottom of the sample causing a loss of material and the increase of porosities within the sample.

4. Conclusions

In this work several carbon-phenolic ablators were manufactured with and without the addition of polyvinylpyrrolidone in different amounts. The infrared spectroscopy, the SEM and XRM analysis and the compression tests of virgin and charred samples allowed to understand how PVP can contribute to the performance of a carbon-phenolic ablator. In particular it was demonstrated that (i) hydrogen bonds are formed between plyvinylpyrrolidone and phenolic resin chains; (ii) the addition of PVP in the carbon-phenolic ablator can modify the micro/nano-structure of the standard carbon-phenolic composite in particular with 20 wt% of PVP; (iii) the mechanical properties can be improved by the PVP addition, in particular this effect is evident for the charred samples as a consequence of the microstructural modification induced by PVP; (iv) the PVP addition can modify the performance of these ablators when exposed to an oxyacetylene flame. When PVP is added to carbon-phenolic ablators, several mechanisms can be active during the heating by an oxyacetylene flame burner: the decomposition of the PVP at about 600 °C with formation of volatile products increases the outgassing and causes a more brittle char residue; the different microstructure causes a lower back temperature and a higher surface temperature, probably because of re-irradiation phenomena. Both SEM and XRM analyses highlight that the amount of PVP addition is more influent on the final microstructure than the different resin-to-solvent ratio adopted in the manufacturing process. The XRM analysis on a PVP-enriched sample after the torch test shows the progression of the pyrolysis within the analyzed sample and gives interesting information about the microstructural modification induced by ablation and pyrolysis phenomena. All data collected highlight the good potentiality of carbon-phenolic ablators manufactured with the addition of other polymers able to influence the microstructure and thus the chemical, mechanical and ablative properties.

Funding

This research did not receive any specific grant from funding agencies in the public, commercial, or not-for-profit sectors.

CRediT authorship contribution statement

Laura Paglia: Writing – original draft, Methodology, Data curation, Conceptualization. **Rita Bottacchiari:** Validation, Investigation. **Flavio Cognigni:** Software, Formal analysis. **Sara Cerra:** Investigation, Data curation. **Virgilio Genova:** Conceptualization. **Marco Rossi:** Supervision. **Ilaria Fratoddi:** Supervision, Conceptualization. **Francesco Marra:** Supervision, Conceptualization. **Giovanni Pulci:** Writing – review & editing, Project administration, Methodology, Conceptualization.

Declaration of competing interest

The authors declare that they have no known competing financial interests or personal relationships that could have appeared to influence the work reported in this paper.

Data availability

Data will be made available on request.

Appendix A. Supplementary data

Supplementary data to this article can be found online at https://doi.org/10.1016/j.matdes.2024.113014.

References

[1] L. Paglia, J. Tirillò, F. Marra, C. Bartuli, A. Simone, T. Valente, G. Pulci, Carbon-phenolic ablative materials for re-entry space vehicles: plasma wind tunnel test and finite element modeling, Mater. Des. 90 (2016) 1170–1180.
[2] L. Paglia, V. Genova, F. Marra, M.P. Bracciale, C. Bartuli, T. Valente, G. Pulci, Carbon-phenolic ablative materials for re-entry space vehicles: Manufacturing and properties, Appl. Energy 42 (2010) 1–11.
[3] O. Uyanna, H. Najafi, Thermal protection systems for space vehicles: a review on technology development, current challenges and future prospects, Acta Astronaut. 176 (2020) 341–356.
[4] F.S. Milos, Y.K. Chen, Ablation and thermal response property model validation for phenolic impregnated carbon ablator, J. Spacecr. Rockets 47 (2019) 786–805.
[5] R.P. Kornfeld, R. Prakash, A.S. Devereaux, M.E. Greco, C.C. Harmon, D.M. Kipp, Verification and validation of the Mars science laboratory/ curiosity rover entry, descent, and landing system, J. Spacecr. Rockets 51 (2014) 1251–1269.
[6] M. Mahzari, R. Beck, H. Hwang, J. Monk, J. Morgan, J. Williams, K. Edquist, Development and sizing of the mars 2020 thermal protection system. AIAA Aviat 2022 Forum (2022) 1–29.
[7] M. Natali, J.M. Kenny, L. Torre, Science and technology of polymeric ablative materials for thermal protection systems and propulsion devices: a review, Prog. Mater. Sci. 84 (2016) 192–275.
[8] L. Paglia, V. Genova, M.P. Bracciale, C. Bartuli, F. Marra, M. Natali, G. Pulci, Thermochemical characterization of polybenzimidazole with and without nano - ZrO2 for ablative materials application, J Therm. Anal. Calorim. 142 (2020) 2149–2161.
[9] L. Paglia, V. Genova, F. Marra, M.P. Bracciale, C. Bartuli, T. Valente, G. Pulci, Manufacturing, thermochemical characterization and ablative performance evaluation of carbon-phenolic ablative materials with nano-Al_2O_3 addition, Polym. Degrad. Stab. 169 (2019) 108979.
[10] J. Xiao, O. Das, R.A. Mensah, L. Jiang, Q. Xu, F. Berto, Ablation behavior studies of charring materials with different thickness and heat flux intensity, Case Stud. Therm. Eng. 23 (2021) 100814.
[11] H.B. Xu, K.Y. Fan, J.X. Yang, X.R. Lian, F.M. He, Z.Y. Li, Design and evaluation of variable porosity charring composite for thermal protection system of reentry vehicles, Case Stud. Therm. Eng. 37 (2022) 102305.

[12] E. Poloni, F. Grigat, C. Duernhofer, D. Leiser, S. Loehle, Assessment of additives for carbon ablators, AIAA SciTech Forum (2022) 1–14.
[13] E. Poloni, F. Bouville, A.L. Schmid, P. Pellisari, V.C. Pandolfelli, M.L.C. Sousa, et al., Carbon ablators with porosity tailored for aerospace thermal protection during atmospheric re-entry, Carbon 195 (2022) 80–91.
[14] F. Grigat, S. Löhle, M. Eberhart, A. Meindl, E. Poloni, R. Ravichandran, et al., Spallation of carbon ablators in arcjet facility experiments, J Thermophys. Heat Transf. 37 (2023) 341–352.
[15] E. Poloni, F. Griga, M. Eberhart, D. Leiser, Q. Sautière, R. Ravichandran, S. Delahaie, C. Duernhofer, I. Hoerner, F. Hugard, S. Loehle, An open carbon–phenolic ablator for scientific exploration, Nature Scientific Report 13 (2023) 13135.
[16] R. Yin, H. Cheng, C. Hong, X. Zhang, Synthesis and characterization of novel phenolic resin/silicone hybrid aerogel composites with enhanced thermal, mechanical and ablative properties, Compos. Part A Appl. Sci. Manuf. 101 (2017) 500–510.
[17] M.M. Seraji, A. Arefazar, Thermal ablation-insulation performance, microstructural, and mechanical properties of carbon aerogel based lightweight heat shielding composites, Polym. Eng. Sci. 61 (2021) 1338–1352.
[18] H. Cheng, C. Hong, X. Zhang, H. Xue, S. Meng, J. Han, Super flame-retardant lightweight rime-like carbon-phenolic nanofoam, Nature Scientific Reports 6 (2016) 33480.
[19] A.Y. Snegirev, M.K. Handawy, V.V. Stepanov, V.A. Talalov, Pyrolysis and combustion of polymer mixtures: exploring additivity of the heat release rate, Polym. Degrad. Stab. 161 (2019) 245–259.
[20] M. Kervran, C. Vagner, M. Cochez, M. Ponçot, M.R. Saeb, H. Vahabi, Thermal degradation of polylactic acid (PLA)/polyhydroxybutyrate (PHB) blends: a systematic review, Polym. Degrad. Stab. 201 (2022) 109995.
[21] J.H. Cheon, E.S. Shin, Assessment of the ablation characteristics of carbon/phenolic composites using X-ray microtomography, Compos. Sci. Technol. 182 (2019) 107740.
[22] G. Pulci, J. Tirillò, F. Marra, F. Fossati, C. Bartuli, T. Valente, Carbon – phenolic ablative materials for re-entry space vehicles : Manufacturing and properties, Compos. Part A 41 (2010) 1483–1490.
[23] L. Paglia, C. Mapelli, V. Genova, C. Bartuli, M.P. Bracciale, F. Marra, I. Fratoddi, G. Pulci, Effect of ceramic nano-particles on the properties of a carbon-phenolic ablator, Polym. Composite 43 (2022) 7345–7359.
[24] F. Cognigni, M. Pasquali, P.P. Prosini, C. Paoletti, A. Aurora, F.A. Scaramuzzo, M. Rossi, X-ray microscopy: a non-destructive multi-scale imaging to study the inner workings of batteries, Hem. Electro. Chem. 10 (2023) e202201081.
[25] D. Dini, F. Cognigni, D. Passeri, A.F. Scaramuzzo, M. Pasquali, M. Rossi, Review—multiscale characterization of Li - ion batteries through the combined use of atomic force microscopy and X - ray microscopy and considerations for a correlative analysis of the reviewed data, J. Electrochem. Soc. 168 (2021) 126522.
[26] A. du Plessis, P. Sperling, A. Beerlink, L. Tshabalala, S. Hoosain, N. Mathe, et al., Standard method for microCT-based additive manufacturing quality control: Porosity analysis, MethodsX 5 (2018) 1102–1110.
[27] M. Bernabale, F. Cognigni, F. Mura, L. Nigro, D. Montanari, M. Rossi, et al., 3D imaging of micro-segregation and corrosion behavior of alloying elements in archaeological artefacts from Motya (Sicily, Italy), Corros. Sci. 211 (2023) 110900.
[28] M. Bernabale, F. Cognigni, L. Nigro, M. Rossi, T. de Caro, C.A. De Vito, A comprehensive strategy for exploring corrosion in iron-based artefacts through advanced multiscale X-ray microscopy, Sci. Rep. 12 (2022) 1–9.
[29] R.S. Bradley, I.K. Robinson, M. Yusuf, 3D X-ray nanotomography of cells grown on electrospun scaffolds, Macromol. Biosci. 17 (2017) 1–8.
[30] F. Cognigni, S. Dinarelli, M. Girasole, G. Longo, G. Fabi, M. Rossi, 3D X-ray microscopy (XRM) investigation of exogenous materials inside mussels' organs, IOP Conf. Ser. Mater. Sci. Eng. 1265 (2021) 012012.
[31] L.A. Feldkamp, Practical cone-beam algorithm, J. Miscosc. 185 (1997) 67–75.
[32] K.E. Parmenter, K. Shuman, F. Milstein, C.E. Szalai, H.K. Tran, D.J. Rasky, Compressive response of lightweight ceramic ablators: phenolic impregnated carbon ablator, J. Spacecr. Rockets 38 (2001) 231–236.
[33] ASTM Interantional C165-07. Standard Test Method for Measuring Compressive Properties of Thermal Insulations (2012).
[34] ASTM International, E285-08. Standard test method for oxyacetyele ablation testing of thermal insulation materials (2020).
[35] G. Pulci, L. Paglia, V. Genova, C. Bartuli, T. Valente, F. Marra, Low density ablative materials modified by nanoparticles addition: manufacturing and characterization, Compos. Part A Appl. S. 109 (2018) 330–337.
[36] F. Marra, G. Pulci, J. Tirillò, C. Bartuli, T. Valente, Numerical simulation of oxy-acetylene testing procedure of ablative materials for re-entry space vehicles, Proc. Inst. Mech. Eng. Part L J. Mater. Des. Appl. 225 (2011) 32–40.
[37] C. Wang, H. Cheng, C. Hong, X. Zhang, T. Zeng, Lightweight chopped carbon fibre reinforced silica-phenolic resin aerogel nanocomposite: facile preparation, properties and application to thermal protection, Compos. Part A Appl. Sci. Manuf. 112 (2018) 81–90.
[38] A. Noparvar-Qarebagh, H. Roghani-Mamaqani, M. Salami-Kalajahi, B. Kariminejad, Nanohybrids of novolac phenolic resin and carbon nanotube-containing silica network: two different approaches for improving thermal properties of resin, J. Therm. Anal. Calorim. 128 (2017) 1027–1037.
[39] S. Salimian, A. Zadhoush, M. Naeimirad, R. Kotek, S. Ramakrishna, A review on aerogel: 3D nanoporous structured fillers in polymer-based nanocomposites, Polym. Compos. 39 (2018) 3383–3408.
[40] A. Rahma, M.M. Munir, A. Khairurrijal, V. Prasetyo, H.R. Suendo, Intermolecular interactions and the release pattern of electrospun curcumin-polyvinyl (pyrrolidone) fiber, Biol. Pharm. Bull. 39 (2016) 163–173.
[41] R. Bryaskova, D. Pencheva, S. Nikolov, T. Kantardjiev, Synthesis and comparative study on the antimicrobial activity of hybrid materials based on silver nanoparticles (AgNps) stabilized by polyvinylpyrrolidone (PVP), J. Chem. Biol. 4 (2011) 185–191.
[42] I. Poljanšek, M. Krajnc, Characterization of phenol-formaldehyde prepolymer resins by in line FT-IR spectroscopy, Acta Chim. Slov. 52 (2005) 238–244.
[43] A.A. Menazea, A.M. Ismail, N.S. Awwad, H.A. Ibrahium, Physical characterization and antibacterial activity of PVA/Chitosan matrix doped by selenium nanoparticles prepared via one-pot laser ablation route, J. Mater. Res. Technol. 9 (2020) 9598–9606.
[44] M.M. Atta, A.M.A. Henaish, A.M. Elbasiony, E.O. Taha, A.M. Dorgham, Structural, optical, and thermal properties of PEO/PVP blend reinforced biochar, Opt. Mater. 127 (2022) 112268.
[45] W.T. Du, Y.L. Kuan, S.W. Kuo, Intra- and intermolecular hydrogen bonding in miscible blends of CO2/epoxy cyclohexene copolymer with poly(vinyl phenol), Int. J. Mol. Sci. 23 (2022) 7018.
[46] I. Sriyanti, M.R. Almafie, Y.P. Nugraha, M.K.N.A. Idjan, J. Jauhari, The morphology of polyvinylpyrrolidone nanofibers containing Anredera cordifolia leaves, Jurnal Hilmia Pendidikan Fisika 10 (2021) 8820.
[47] N.N. Sedeh, M. Entezam, S.H. Jafari, H.A. Khonakdar, M. Abdouss, Morphology, drug release behavior, thermal, and mechanical properties of poly(ethylene oxide) (PEO)/poly(vinyl pyrrolidone) (PVP) blends, J. Appl. Polym. Sci. 135 (2018) 46403.
[48] M.A. Morsi, A. Rajeh, A.A. Menazea, Nanosecond laser-irradiation assisted the improvement of structural, optical and thermal properties of polyvinyl pyrrolidone/carboxymethyl cellulose blend filled with gold nanoparticles, J. Mater. Sci. Mater. El. 30 (2019) 2693–2705.
[49] D. Thavarajah, P. Thavarajah, A. Sarker, M. Materne, G. Vandemark, R. Shrestha, et al., A global survey of effects of genotype and environment on selenium concentration in lentils (Lens culinaris L.): Implications for nutritional fortification strategies, Food Chem. 125 (2011) 72–76.
[50] S. Baccaro, L.A. Pajewski, G. Scoccia, R. Volpe, J.M. Rosiak, Mechanical properties of polyvinylpyrrolidone (PVP) hydrogels undergoing radiation, Nucl. Instrum. Meth. B 105 (1995) 100–102.
[51] F. Cardona, A.L. Kin-Tak, J. Fedrigo, Novel phenolic resins with improved mechanical and toughness properties, J. Appl. Polym. Sci. 123 (2012) 2131–2139.
[52] N. Azeez Betti, Thermogravimetric analysis on PVA / PVP blend under air atmosphere, Eng. Technol. J. 34 (2016) 2433–2442.
[53] L. Paglia, V. Genova, J. Tirillò, C. Bartuli, A. Simone, G. Pulci, F. Marra, Design of new carbon - phenolic ablators : manufacturing, plasma wind tunnel tests and finite element model rebuilding, Appl. Compos. Mater. 28 (2021) 1675–1695.
[54] J. Huang, J. Guo, H. Huang, Q. Wang, W. Li, Components of thermal protection mechanism of carbon/phenolic composites exposed to severe aerodynamic heat, Polym. Compos. 44 (2023) 136–147.
[55] H. Zhao, L. Chen, J. Yun, L. Tang, Z. Wen, X. Zhang, et al., Improved thermal stabilities, ablation and mechanical properties for carbon fibers/phenolic resins laminated composites modified by silicon-containing polyborazine, Eng. Sci. 2 (2018) 57–66.
[56] R. Sha, X. Cheng, J. Dai, Y. Zu, Y. Zeng, J. Sha, Lightweight phenolic resin aerogel with excellent thermal insulation and mechanical properties via an ultralow shrinkage process, Mater. Lett. 324 (2022) 132626.